2D crustal scale velocity models for western Norway derived from receiver function analysis and trans-dimensional inversion

GEOLOGICAL SURVEY OF NORWAY
- NGU -

Marco Brönner[a] & Claudia Pavez[a]

a. Geological Survey of Norway (NGU), Trondheim, Norway

A. Introduction

Receiver functions are the deconvolved P to S conversions of tele-seismic waves at sub-horizontal crustal-upper mantle discontinuities (**figure 1**). Because of this natural conversion, they constitute a very useful technique to find detectable interfaces such as intra-crustal discontinuities or major transition zones, like the Mohorovicic discontinuity (Zhu & Kanamori, 2000). Lately, they have been used as input data in order to calculate velocity models, treating the inversion process as a trans-dimensional problem, which means that the thickness and the number of layers are also unknown variables (Piana Agostineti & Malinverno, 2010; Bodin et al., 2012).

Seismic tomography, active source seismic refraction and receiver function analysis have shown the resultant litospheric structure under Southern Norway, showing in general clear Moho discontinuities and non-pronounced intracrustal low and high velocity anomalies. However, some flat-lying structures near the Moho and Moho offsets inferred for example by Stratford & Thybo (2011b) and Svenningsen et al. (2007), have not been fully explained so far.

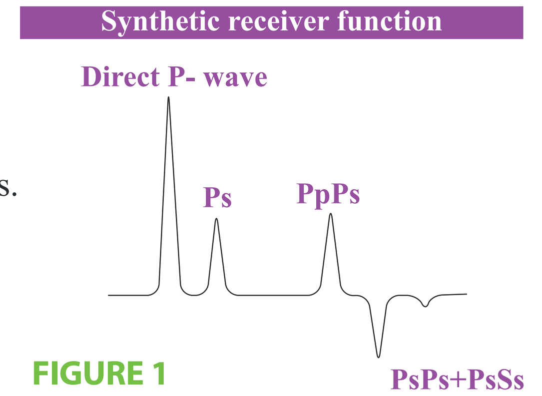

FIGURE 1

B. Outline

We present a receiver function analysis along two profiles located in north- and southwestern Norway. One of them, the northern profile, is crossing the entire Western Gneiss Region (Figure 2). In order to understand and better image the crustal structure and the Moho transition zone, including complex sub-Moho structures, we used the tele-seismic data, recorded by twelve broadband seismic stations, which constituted a temporary array deployed by the University of Aarhus as part of the GEOFON global network (Figure 2). Further, using the Hκ technique (Zhu & Kanamori, 2000), we calculated the Moho topography and the Vp/Vs ratios under each station in order to compare the method with previous results as well as to constraint the local geology. At last, a 1D S-wave velocity model based on Markov chains and the Monte Carlo approach (Rj-McMC inversion) was calculated (Bodin et al., 2012) in order to observe the main velocity interfaces that characterize the area, including for example discontinuities as well as the crustal-mantle transition zone and its features.

C. Geological setting

The Caledonian orogeny (490-390 Ma) was one of the major tectonic events on the Fennoscandian shield, formed during the collision between Baltica and Laurentia. During this period, allochthonous nappes were thrusted onto Fennoscandian basement rocks from the west, forming four well identified nappe units, from which three are present in southern Norway (Stratford & Thybo, 2011b): the upper, middle and lower allochton Caledonides Western Norway is dominated by the Western Gneiss Region (WGR; Figure 2), an area that was strongly reworked during the Caledonian orogeny. It is composed of high to ultra-high pressure rocks, including eclogites in the northwest, indicating ultra-high pressure depths around 425-400 Ma (Hacker et al., 2010). In fact, subduction down to 100 km depth in the east to 20 km in the east, suggests westward subduction of the basement and portions of the allochthons units (Walsh et al., 2007). During post-orogenic collapse in the late-Caledonian (Hacker et al., 2010), the ultra-high pressure rocks of the WGR were exhumed (Walsh et al., 2007).

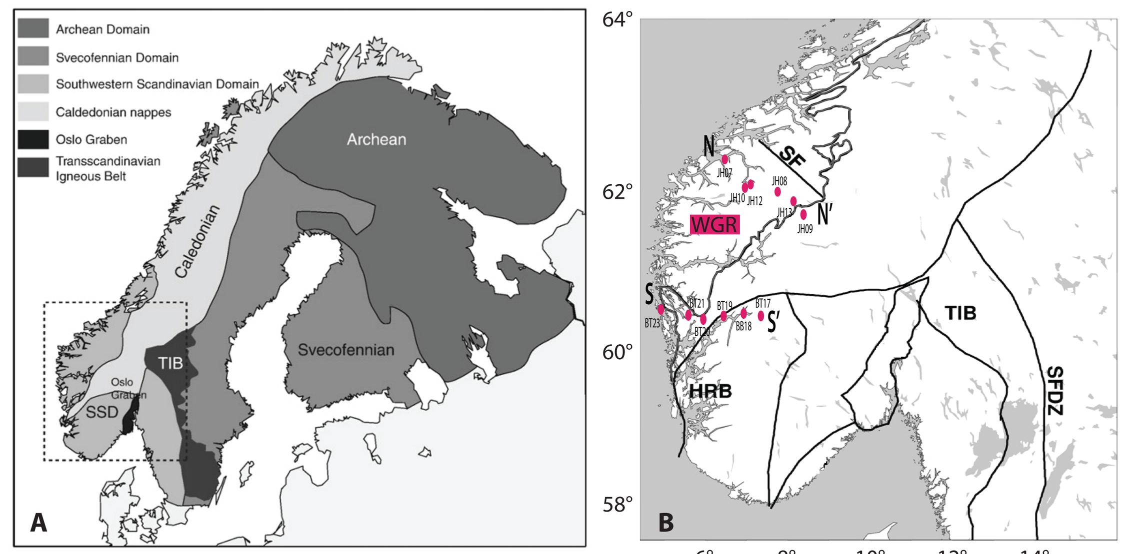

FIGURE 2

A) Map containing the three main crustal domains at the Fennoscandian shield (modified from Stratford & Thybo., 2011) and B) the outline of southern Norway showing some of the main geological units close to the study area. The seismic stations are marked with pink dots. Northern (NN') and southern (SS') profiles are also shown.

WGR - Western Gneiss Region
HRB - Hardangervidda-Rogaland Block
SFDZ - Sveconorwegian Frontal Deformation Zone

D. Seismic network & data

Seismic stations are part of the GEOFON/Aarhus temporary network composed of 30 three-component and continuous recording stations which were operating for different periods between 2002-2005 (Table 1). The seismographs were installed in private properties far away from sources of noise (Svenningsen et al., 2007). In this research, just the recordings of twelve of them were used, according to our study area (Figure 2 & Table 1). Seismic data were obtained from the GEOFON Data Center, which is available online, using their web3DC service for selection and extraction. A total of 801 earthquakes with minimum magnitude of Mw=5.5 were recorded during that period, from which those with epicentral distances between 30° - 90° were kept for further analysis (Table 1).

After visual inspection and quality filters applied, just the events with high signal quality were considered. Using these criteria, the number of accepted events varies from one station to another.

Station	Latitude	Longitude	Elevation (m)	Total events vs selected events
JH07	62.437	6.432	130	154/ 23
JH10	62.082	6.891	198	106/ 46
JH12	62.083	7.022	401	106/ 39
JH08	62.016	7.665	930	159/ 14
JH13	61.904	8.034	527	92/ 31
JH09	61.726	8.280	780	161/ 43
BT23	60.490	4.933	32	114/ 25
BT21	60.439	5.575	122	116/ 33
BT20	60.388	5.908	396	129/ 47
BT19	60.415	6.386	34	117/ 59
BB18	60.467	6.859	101	121/ 29
BT17	60.423	7.273	721	114/ 44

TABLE 1

Station names, location and elevation. The last column shows the number of accepted events for receiver function calculation.

E. Methodology

1. Receiver function calculation

After the preprocessing, the RFs were calculated using the Iterative Time Domain Deconvolution (Ligorria & Ammon, 1999), available in the CPS package (Hermann, 2013) for the radial component. After testing, the selected Gaussian filter was set to a= 2.0, corresponding to a gain of 0.1 at approximately 1 Hz. This selection allowed us to remove the remanent high frequency noise and to better define the spikes of interest. The calculation process consisted of 1000 iterations and a tolerance error equal to 0.0001%, which allowed us to reproduce higher percentages of the signal.

2. HK stacking calculation

Individual receiver functions were used in the HK subroutine available for SAC (Helffrich et al., 2013). This routine considers as inputs the individual ray parameters (p) per event and a Vp average crustal velocity of 6.2 km/s, minimizing the RMS during the HK stacking process. The weighting factors were 0.5, 0.4 and 0.1, respectively, representing the direct P-to-S conversion, Ps, and the reverberations PpPs and PsPs + PpSs. By last, the selected ratio ranges were 20 < H < 50 and 1.5 < K< 2.2 for the crustal thickness and Vp/Vs ratio, respectively.

3. Transdimensional inversion

The average RF considering all selected events was used as an entry data vector in the Rj-rf code. This is an open-source software for inversion of seismic receiver functions to obtain the 1D shear wave velocity structure under each station using the reversible jump Markov chain Monte Carlo algorithm (Bodin et al., 2012). Initially, it is possible to fix the number of iterations (5000), the burn-inperiod (1000), and the maximum number ofpartitions of different velocities (15).

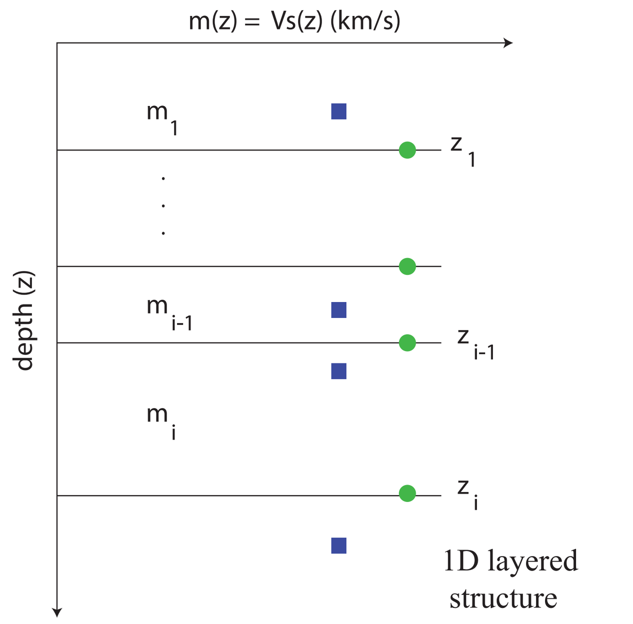

FIGURE 3

Schematic representation of a one-dimensional transdimensional model applied to receiver function inversion. m represents the velocity, which is the model unknown, but additionally the number of layers and their thicknesses are also a variable.

F. Results: HK stacking & transdimensional inversion

Northern profile (NN')			Southern profile (SS')		
Station	Moho depth	Vp/Vs	Station	Moho dpth	Vp/Vs
JH07	49.76 ± 0.18	1.90 ± 0.05	BT23	30.51± 1.71	1.54 ± 0.05
JH10	44.20 ± 0.46	1.85 ± 0.01	BT21	31.63± 1.10	1.69 ± 0.06
JH12	39.03 ± 0.54	1.81 ± 0.02	BT20	30.99± 0.34	1.50 ± 0.04
JH08	37.77 ± 0.60	1.66 ± 0.02	BT19	34.97± 0.39	1.89 ± 0.01
JH13	41.17 ± 0.66	1.69 ± 0.02	BB18	38.82± 0.37	1.62 ± 0.02
JH09	39.21 ± 1.12	1.69 ± 0.04	BT17	36.69± 0.90	1.61 ± 0.03

TABLE 2 *Moho depths and Vp/Vs parameters for northern and southern profiles*

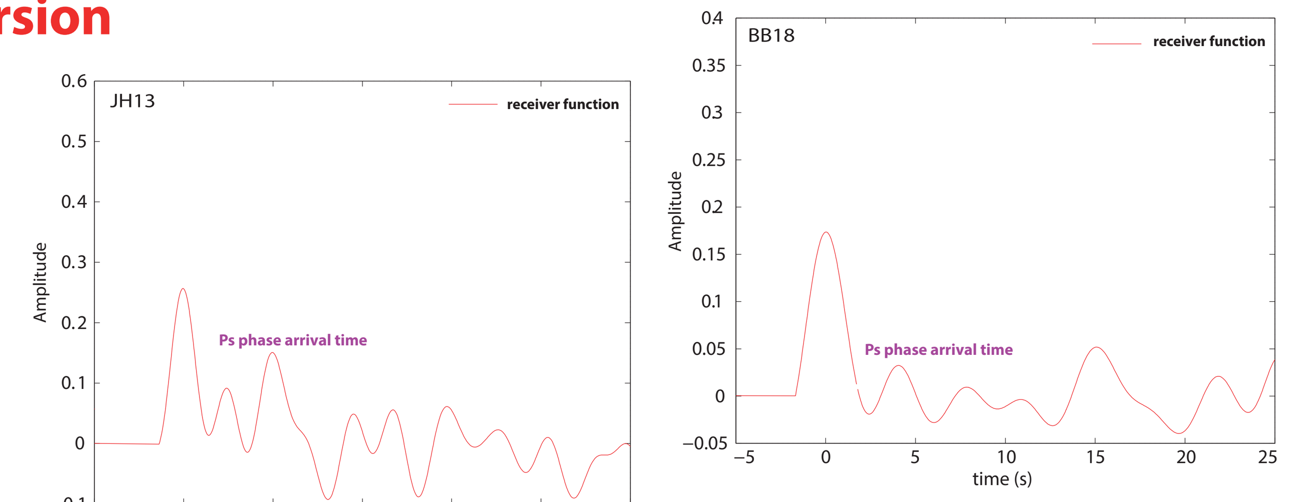

FIGURE 4 *Receiver function examples for northern (JH13) and southern profiles (BB18)*

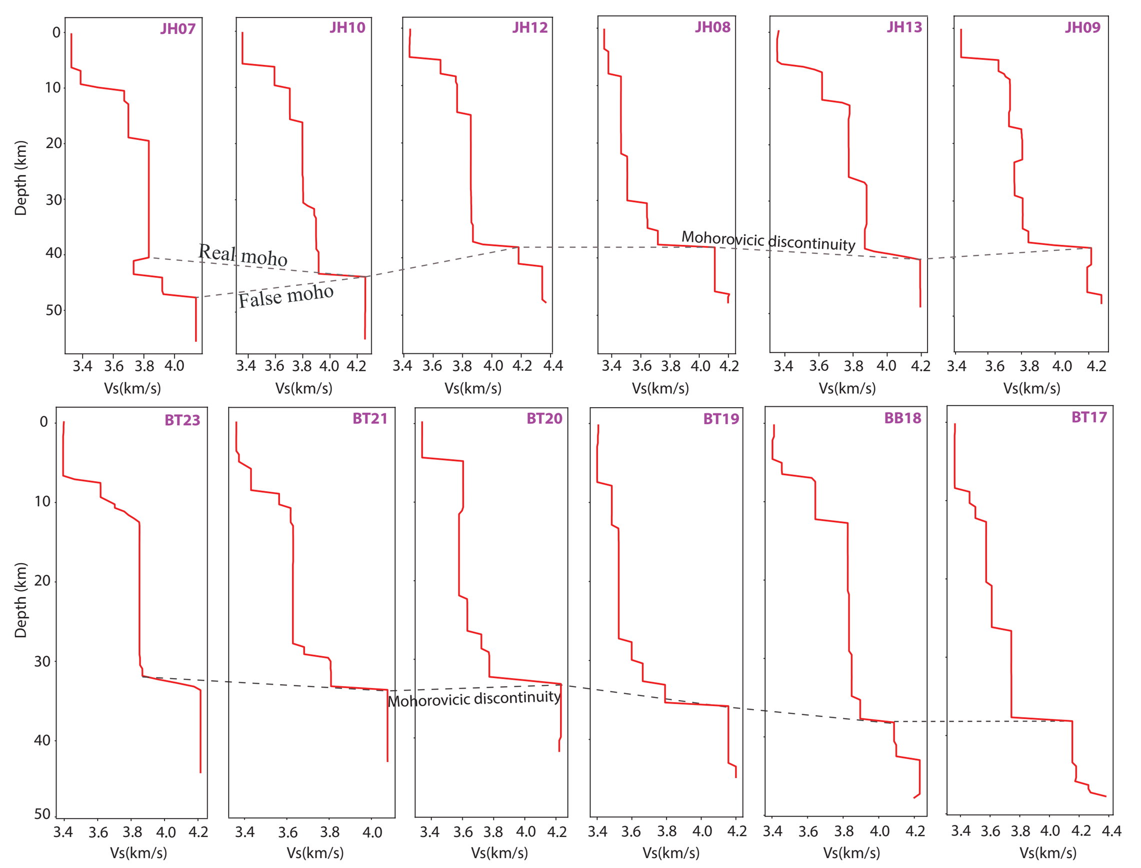

FIGURE 5 *Posterior ensemble showing the 1D-S wave velocity model for all stations located in the northwestern and southwestern profiles*

The earliest Ps arrivals (~2.5 – 3.5 s) are observed for stations BT23, BT21 and BT20, where the thinnest crust was found (Table 2). The crust becomes thicker under stations BT19, BB18 and BT17, which is also reflected in the Ps arrival times (~4.0 – 5.0 s), with a Moho depth varying from 35 to 39 km. In the velocity model, several intracrustal discontinuities could be observed. The velocity transitions are smooth for stations BT21, BT19 and BT17. On the contrary, sharp interfaces are clearly identifiable in the first 10 km depth under stations BT23, BT20 and BB18. The most patent interface is related with the Mohorovicic discontinuity (Figure 5). In all the cases, the velocity changes from the crust to the adjacent upper mantle goes from 3.8 to 4.2 km/s (Figure 5), as was also observed in the velocity models of nearby stations of the MAGNUS network (Maupin & Kolstrup, 2013).

For stations JH07, JH10 and JH12 the Ps arrival times are ranging between 7.5 to 6.0 s. from west to east, indicating a very thick crust near to the coast. Regarding stations JH08, JH13 and JH09, our findings exhibit in general Ps arrival times around 5 s.

In relation to the velocity model for the northwestern profile (Figure 5), sharp discontinuities can be observed between 5 to 10 km depth for all seismic stations, with exception of JH08. In addition, a high velocity anomaly can be observed between ~20-24 km depth under station JH09. As could be noticed for the southern stations, the Mohorovicic discontinuity is the most evident interface along the profile. Velocities to the lower crust to the immediately upper mantle are ranging from ~3.8 to 4.1 or 4.2 km/s. Under station JH07, the average velocity model shows an extensive crustal-mantle transition area: a low velocity zone is observed between ~ 40 - 43 km depth, after which the interface could be divided in two different velocity segments from ~43 to 46 km depth and from ~46 to 49 km depth (Figure 5).

2D velocity models and conceptual sketch

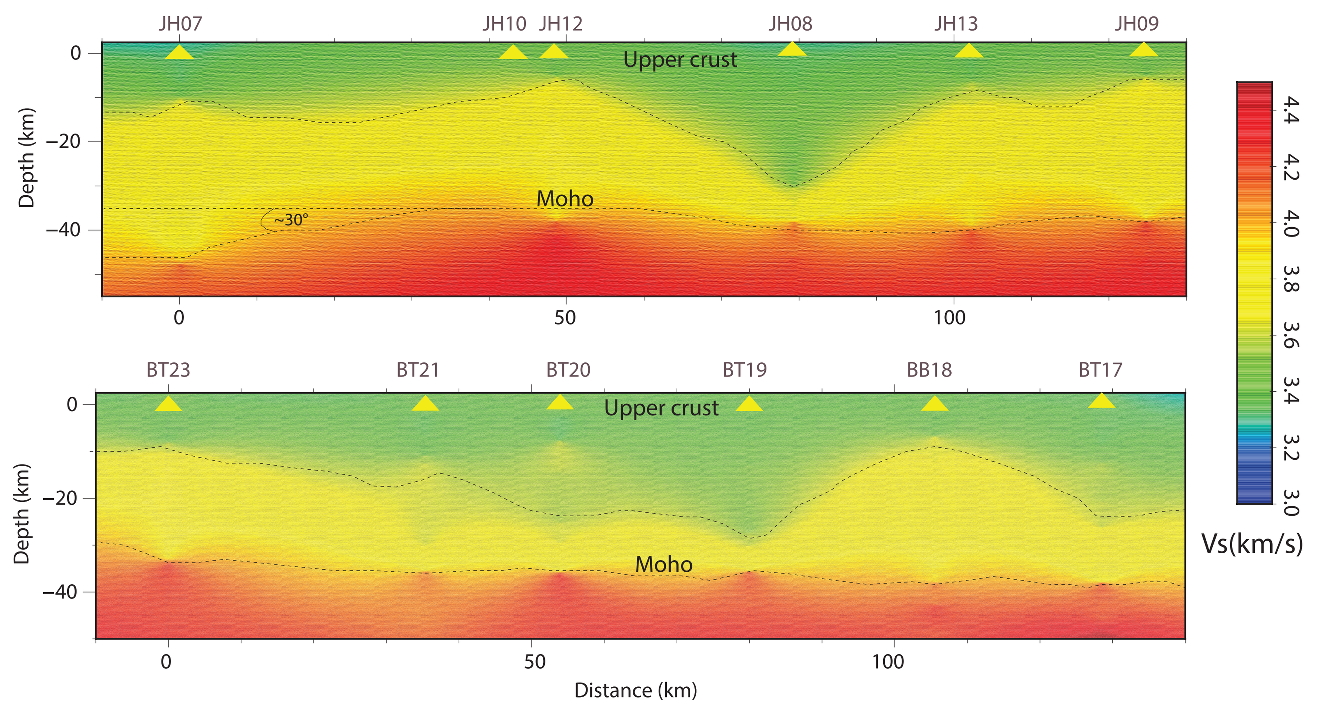

FIGURE 6 *2D Vs-velocity model for NN' and SS' profiles. Seismic stations are shown with yellow triangles, and the delimitations between the upper and middle crust and the Moho discontinuity are marked with black dotted lines.*

The most noticeable feature regarding the Moho depths and velocity models is the very thick crust obtained under stations JH07 & JH06. In these cases, our results exhibit significant differences with previous models already published which indicate a crust between 5 to 16 km less.The difference between our results and previous research at the westernmost stations of the northern profile could be explained bearing in mind the presence of a paleo-structure that has been formerly documented and explained as a flat lying reflector in the upper mantle close to the Mohorovicic discontinuity, with depths varying between 46 ± 3 km (Svenningsen et al. 2007; Stratford & Thybo, 2011b; Kolstrup & Maupin, 2013).

This paleo-structure is observable from ~40 to ~49 km depth in the 1D velocity model (Figure 5), where the velocity transitions are interpreted as the'real' Moho depth, at ~40 km depth, a mantle wedge characterized by a low velocity zone, the presence of an old crustal segment from Baltica and finally the upper mantle, interface that was interpreted by the model as the largest velocity transition (Figure 5 & Figure 6). This structure extends almost 70 km inland from station JH07, which coincides with the westernmost border of the Western Gneiss Region (Figure 2) and the 2D projection shows a dipping angle of ~30° to the northwest (Figure 6).

This hypothesis is strongly supported by the high Poisson's ratios (Table 2) that are registered under the westernmost stations of the northern profile. The subduction processes that involved ultra-high temperature and pressure conditions may have caused a phase transition from mafic rocks to eclogite facies (Hacker et al. 2010), transforming the old subducted crust into mantle-like rocks, increasing the Poisson ratio with respect to a tectonically stable crust (Qiang et al., 2010). On average, the Poisson's ratio increases with the age of the crust (Zandt & Ammon, 1995) and in this case the continental collision process suggest an intermediate-to-mafic composition. Additionally, very high Poisson ratios have been previously connected with the presence of melts/fluids that according our results should be in the proposed mantle wedge (Hajra et al., 2019).

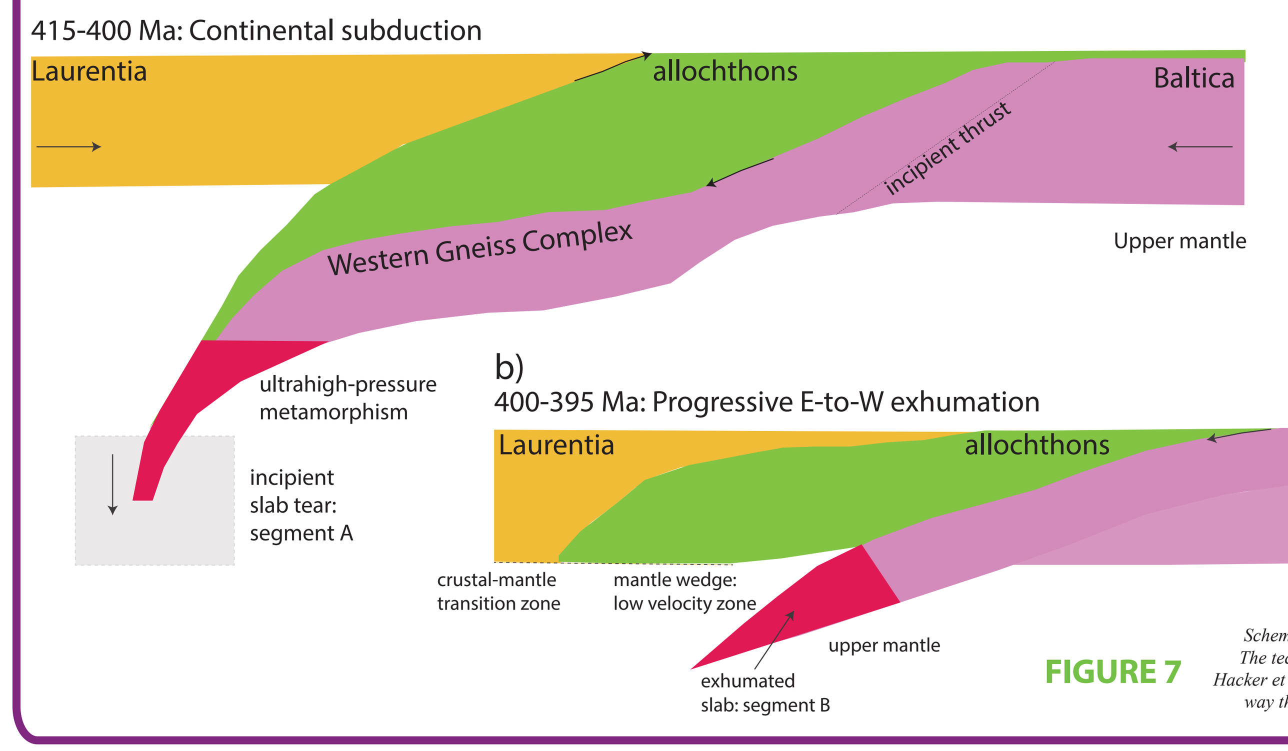

An schematic model linked to the 1D velocity results (Figure 5) is presented according to the tectonic summary made by Hacker et al., (2010) (Figure 7). At the beginning, between 415-400 Ma, the subducted plate could be divided in two different segments (A and B): an incipient slab tear and the remnant crust that was previously exhumated lately between 400 – 395 Ma (Hacker et al. 2010). The paleo-slab corresponding to the exhumated crust formed a mantle wedge (low velocity zone) that still remains under the northern profile. The oldest crust (Figure 7) even now preserves its own velocity transient, after which the upper mantle can be found with S-wave velocities going beyond to 4.1 km/s.

FIGURE 7 *Schematic tectonic model that explains the results obtained from the 1D and 2D velocity models. The tectonic stages and the metamorphism information were obtained from the diagrams made by Hacker et al. 2010 according to his research and references there in. a) Stage 1, which shows in a simple way the main tectonic elements involved in the continental collision. b) Stage 2, showing how the exhumation process could modify the crustal mantle transition zone.*

This project was funded by the Chilean state through the Postdoctoral fellowship 'Postdoctorado en el extranjero Becas Chile 2019' project number 7420005 'Seismic Imaging using Norwegian Earthquakes'. Additionally, this research was done thanks to the support of the Norges Geologiske Undersøkelse (NGU). The authors also thanks to the GFZ/GEOFON Data Center to freely provide the data that made this research possible

Main references & software:

Bodin, T., Sambridge, M., Tkalčić, H., Arroucau, P., Gallagher, K. & Rawlinson, N. 2012. Transdimensional inversion of receiver functions and surface wave dispersion. J. Geophys. Res., 117, B02301
Hacker, B.R., Andersen, T.B., Johnston., S., Kylander-Clark, A.R.C., Peterman, E.M., Walsh, E.O., Young, D. 2010. High-temperature deformation during continental-margin subduction & exhumation: The ultrahigh-pressure Western Gneiss Region of Norway. Tectonophysics 480. 149-171.
Helffrich, G., Wookey, J., Bastow, I. 2013: The Seismic Analysis Code: A Primer and User's Guide. Cambridge University Press, United Kingdom
Hermann, R. 2013: Computer Programs in Seismology: An evolving tool for instruction and research. Seismological Research Letters 84. 1081–1088.
Ligorria, J.P., Ammon, CJ. 1999. Iterative deconvolution and receiver-function estimation. Bulletin of Seismological Society of America 89 (5). 1395–1400.
Kolstrup, M.L., Maupin, V. 2013: A Proterozoic boundary in Southern Norway revealed by joint-inversion of P-receiver functions and surface waves. Precambrian Research. 238. 186-198.
Piana Agostinetti, N. & Malinverno, A. 2010. Receiver function inversion by trans-dimensional Monte Carlo sampling. Geophys. J. Int. 181. 858–8
Stratford, W. & Thybo, H. 2011b. Seismic structure and composition of the crust beneath the southern Scandes, Norway. Tectonophysics 502. 364–382.
Qiang, X., JunMeng, Z., ZhongXiong, C., ShunPing, P., HongBing, L. 2009. Moho offset beneath the central Bangong-Nujiang suture of Tibetan Plateau.
Svenningsen, L., Balling, N., Jacobsen, B.H., Kind, R., Wylegalla, K., Schweitzer, J. 2007. Crustal root beneath the highlands of southern Norway resolved by teleseismic receiver functions. Geophys. J. Int. 170. 1129–1138.
Walsh, E.O., Hacker, B.R., Gans, P.B., Grove, M., Gehrels, G. 2007. Protolith ages and exhumation histories of ultrahigh pressure rocks across the Western Gneiss Region, Norway. GSA bulletin 119. 289-301.
Zandt, G. & Ammon, C.J. 1995. Continental crust composition constrained by measurements of crustal Poisson's ratio. Nature. Vol. 374. Pp 152-154.
Zhu, L. & H. Kanamori. 2000: Moho depth variation in southern California from teleseismic receiver functions. Journal of Geophysical Research, 105, 2969–2980.

QGIS

Google Earth

SAC

MATLAB